

See discussions, stats, and author profiles for this publication at: <https://www.researchgate.net/publication/274255992>

# A Light-Triggered Switch Based on Spiropyran/Layered Double Hydroxide Ultrathin Films

ARTICLE *in* THE JOURNAL OF PHYSICAL CHEMISTRY C · MARCH 2015

Impact Factor: 4.77 · DOI: 10.1021/acs.jpcc.5b00753

---

CITATIONS

2

READS

56

## 8 AUTHORS, INCLUDING:



Shulin Wan

Beijing University of Chemical Technology

5 PUBLICATIONS 9 CITATIONS

[SEE PROFILE](#)



Meizhen Yin

Beijing University of Chemical Technology

114 PUBLICATIONS 609 CITATIONS

[SEE PROFILE](#)

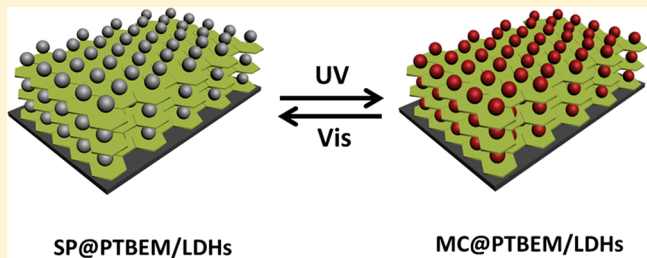
# A Light-Triggered Switch Based on Spiropyran/Layered Double Hydroxide Ultrathin Films

Zhixiong Li, Shulin Wan, Wenying Shi, Min Wei,\* Meizhen Yin,\* Wantai Yang, David G. Evans, and Xue Duan

State Key Laboratory of Chemical Resource Engineering, Beijing Laboratory of Biomedical Materials, Beijing University of Chemical Technology, Beijing 100029, People's Republic of China

## Supporting Information

**ABSTRACT:** Intelligent photoresponsive materials have shown broad applications in antiflare, coating, biomarker, information storage, and optical devices. This article describes the design and fabrication of a photoresponsive switch via a two-step procedure: (i) spiropyran (SP) as a chromophore was encapsulated within a block copolymer (poly(*tert*-butyl acrylate-*co*-ethyl acrylate-*co*-methacrylic acid), PTBEM) to produce SP@PTBEM micelle; (ii) an organic–inorganic ultrathin film (UTF) was prepared by layer-by-layer (LBL) self-assembly of the negatively charged SP@PTBEM micelle and positively charged MgAl-layered double hydroxide (LDH) nanoplatelets (denoted as (SP@PTBEM/LDHs)<sub>n</sub> UTF; *n* represents the bilayer number). Fluorescence spectroscopy and scanning electron microscopy (SEM) indicate a uniform and ordered layered structure with stepwise growth. The resulting (SP@PTBEM/LDHs)<sub>n</sub> UTF serves as an intelligent photoresponsive switch based on the structural transformation between SP and merocyanine (MC), which is triggered by alternate irradiation of UV/visible light. In addition, the UTF exhibits a high reversibility and photostability, which can be potentially used in photochromic materials and devices.



## 1. INTRODUCTION

Light-triggered switches undergo a well-accepted mechanism in which chemical species can be transformed upon exciting in different wavelength. They have evoked considerable interest owing to fast response, high quantum yields and stability, which have been extensively utilized in the fields of logic gate, optical devices, ionic sensors, and advanced bioimaging.<sup>1–5</sup> Spiropyran (SP) compounds, with superior photochemical and photophysical properties, are promising photoresponsive candidates in fluorescence sensors and switches.<sup>6–8</sup> Colorless ring-closed SP undergoes UV light-induced ring-opening reactions, yielding the corresponding isomeric merocyanine (MC), which absorbs strongly in the visible light range 500–620 nm; the back-conversion from MC to SP occurs thermally at relatively low rates but is significantly accelerated by visible-light illumination.<sup>9</sup> Although the photoresponsive behavior of SP has been widely studied in liquid phase,<sup>10–13</sup> the investigation on solid materials or devices is rather limited and unsatisfactory. The immobilization process normally suffers from the loss in dye sensitivity (fluorescence quenching) and stability (photobleaching over time).<sup>14–16</sup> Therefore, it is essential to explore new materials and approaches for the fabrication of SP-based solid optical switches with fast response, high stability, and good workpiece ratio.

Recently, inorganic–organic hybrid materials with ordered nanostructure have attracted much attention by taking advantage of individual merits as well as their synergistic effect.

Layered double hydroxides (LDHs) are one type of inorganic layered materials, whose structure can be expressed as general formula  $[M^{II}_{1-x}M^{III}_x(OH)_2] (A^{n-})_{x/n} \cdot mH_2O$  ( $M^{II}$  and  $M^{III}$  are divalent and trivalent metal ions respectively and  $A^{n-}$  is an anion).<sup>17–20</sup> By virtue of their versatility in chemical composition and morphological architecture, LDHs have been widely used in organic–inorganic functional materials.<sup>21–26</sup> Specially, positively charged LDHs nanosheets and nanoplatelets can be employed to assemble with anionic chromophores,  $\pi$ -conjugated polymers and dyes to obtain photofunctional ultrathin films (UTFs).<sup>27–31</sup> However, only anionic chromophores are available in this approach, which limits the application of a broad spectrum of neutral species such as SP materials. This inspires us to take the challenge of constructing SP-LDHs UTFs, so as to obtain solid light-triggered switches.

In this work, we report the design and fabrication of a photoresponsive UTF switch involving the following two steps: (i) encapsulation of SP within an amphiphilic block copolymer (PTBEM) to give (SP@PTBEM) micelle; and (ii) self-assembly of the negatively charged (SP@PTBEM) micelle and positively charged LDHs nanoplatelets to obtain the final (SP@PTBEM/LDHs)<sub>n</sub> UTFs. A uniform and stepwise growth

Received: January 24, 2015

Revised: March 18, 2015

Published: March 19, 2015



of the UTFs is observed by fluorescence spectroscopy and SEM. The resulting UTFs act as a photoinduced switch with fast response owing to the SP-MC transformation, triggered by alternate irradiation of UV-visible light. The amphiphilic copolymer PTBEM is essential for the fabrication of (SP@PTBEM/LDHs)<sub>n</sub> UTFs: the hydrophobic terminal combining with SP is located in the micelle core; while the hydrophilic terminal with negative charge interacts with LDHs nanoplatelets for the construction of UTFs. The PTBEM micelle offers a hydrophobic and flexible microenvironment for the accommodation of SP with fast SP-MC transformation and satisfactory sensitivity. In addition, the presence of LDHs contributes to the enhanced reversibility and photostability, which would guarantee the practical application of this hybrid UTF.

## 2. EXPERIMENTAL SECTION

**2.1. Reagents and Materials.** 4-Hydrazinobenzoic acid hydrochlorid (97%), 3-methyl-2-butanone (98%), 4-methylphenylhydrazine hydrochloride (98%), and 2-hydroxy-5-nitrobenzaldehyde (98%) were purchased from Alfa Aesar and used without further purification. All solvents were dried prior to use with appropriate drying agents. Analytical thin layer chromatography (TLC) was carried out on Yantai chemical industry silica gel plates and visualized by UV. Poly(*tert*-butyl acrylate-*co*-ethyl acrylate-*co*-methacrylic acid) [ $\text{CH}_2\text{CH}[\text{CO}_2\text{C}-(\text{CH}_3)_3]_x[\text{CH}_2\text{CH}(\text{CO}_2\text{C}_2\text{H}_5)]_y[\text{CH}_2\text{C}(\text{CH}_3)(\text{CO}_2\text{H})]_z$  (PTBEM), and poly dimethyldiallylammonium chloride (PDDA,  $M_w = 100\,000\text{--}200\,000$ ) was purchased from Sigma-aldrich development Co. Ltd. Analytical grade  $\text{Mg}(\text{NO}_3)_2 \cdot 6\text{H}_2\text{O}$ ,  $\text{Al}(\text{NO}_3)_3 \cdot 9\text{H}_2\text{O}$ ,  $\text{NaOH}$  and ethylene glycol monobutyl ether ( $(\text{CH}_3(\text{CH}_2)_3\text{OCH}_2\text{CH}_2\text{OH})$ ) were purchased from Beijing Chemical Co. Ltd. All other chemicals were analytical grade and used as received without further purification. Deionized water was used throughout the experimental process.

**2.2. Preparation of Spiropyran ( $\text{C}_{20}\text{H}_{20}\text{N}_2\text{O}_3$ ).** See details in the Supporting Information.

**2.3. Preparation of SP@PTBEM micelle.** The SP@PTBEM micelle was synthesized by aliquid synthesis method. The SP was dissolved in ethylene glycol monobutyl ether (GME) solvent to give a solution (1 mg/mL); 2 mL of SP in GME solution was added dropwise into a 38 mL of PTBEM micelle solution (0.368 mg/mL, pH = 7.0, adjusted by 0.1 M NaOH solution) with ultrasonic treatment, keeping the pH value of the final SP@PTBEM micelle at 7.0.

**2.4. Preparation of (SP@PTBEM/LDHs)<sub>n</sub> UTFs, (SP@PTBEM/PDDA)<sub>n</sub> UTFs, and SP@PTBEM Drop Film.** The synthesis of MgAl-LDHs colloidal suspension was prepared according to the separate nucleation and aging steps (SNAS) method reported by our group. The quartz substrate was first cleaned in concentrated  $\text{H}_2\text{SO}_4/\text{H}_2\text{O}_2$  (30%) (7:3, v/v) for 30 min and then washed with pure water. The cleaned substrate was dipped into a PDDA solution (1.0 g/L) for 20 min, then thoroughly rinsed with water and dried in air, so as to obtain a positively charged surface. The pretreated substrate was immersed into the negatively charged SP@PTBEM micelle for 10 min followed by washing and then treated with a colloidal suspension (1 g/L) of LDHs nanoplatelets for another 10 min and washed thoroughly. The multilayer (SP@PTBEM/LDHs)<sub>n</sub> UTFs were fabricated by the alternate deposition of SP@PTBEM micelle and LDHs nanoplatelets for  $n$  cycles. As reference samples, the (SP@PTBEM/PDDA)<sub>n</sub> UTFs were fabricated with the same procedure except replacing LDHs

nanoplatelets with PDDA solution (1.0 g/L). Pristine SP@PTBEM film was prepared by a drop-casting method, which was prepared by dropping 200  $\mu\text{L}$  of SP@PTBEM micelle solution (SP: 0.05 g/L; PTBEM: 0.35 g/L) onto a 3 cm<sup>2</sup> substrate and dried at 60 °C for 30 min.

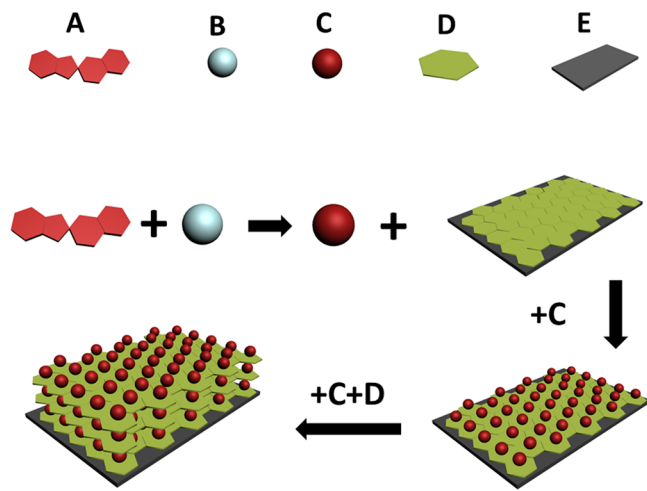
**2.5. Sample Characterization.** The fluorescence spectra were performed on a RF-5301PC fluorospectrophotometer under identical conditions with an excitation wavelength of 365 nm. The fluorescence lifetime was fitted by recording the fluorescence decay curve with an Edinburgh Instruments FL 900fluorimeter, with the excitation at 365 nm and detection wavelength at the maximal photoemission. The percentage contribution of each lifetime component to the total decay curve was calculated by the Edinburgh F900 instrument software. Photoluminescence quantum yield (PLQY) was measured using a HORIBA JobinYvonNanolog FL3-2 iHRSpectrofluorimeter. A Zeiss Supra 55 scanning electron microscope (the accelerating voltage applied was 20 kV) was used to investigate the surface morphology of UTFs. X-ray diffraction (XRD) patterns of the films were recorded using a Rigaku 2500VB2+PC diffractometer using the Cu K $\alpha$  radiation ( $\lambda = 1.541844 \text{ \AA}$ ) at 40 kV and 50 mA with the step-scanned mode in 0.04° (2 $\theta$ ) per step and count time of 10 s/step in the range from 3 to 70°. X-ray photoelectron spectra (XPS) were recorded on a Thermo VGESCALAB250 X-ray photoelectron spectrometer at a pressure of  $2 \times 10^{-9}$  Pa using Al K $\alpha$  X-ray as the excitation source. Fluorescence microscopy image was recorded on a Broadband Confocal and Multiphoton Microscope (TCS SPSMP) with a Two-photon near-infrared pulse laser on 730 nm at 5 frames/s.

## 3. RESULTS AND DISCUSSION

**3.1. Fabrication of (SP@PTBEM/LDHs)<sub>n</sub> UTFs.** Spiropyran was synthesized according to a standard Fisher-ring reaction (Supporting Information Figures S1–S4 and Schemes S1–S2), which undergoes a structural transformation from non-fluorescent closed-ring SP to red-fluorescent open-ring MC triggered by UV, and subsequently reverts back to SP by visible light.<sup>32–35</sup> However, both the neutral property and indissolvability in water are big obstacles for its assembly with LDHs nanoplatelets. The amphiphilic copolymer PTBEM plays a key role in the preparation of (SP@PTBEM/LDHs)<sub>n</sub> UTFs: the hydrophobic terminal combining with SP is located in the micelle core; while the hydrophilic terminal with negative charge interacts with LDHs nanoplatelets for the construction of UTFs. Scheme 1 shows the detailed assembly process of the (SP@PTBEM/LDHs)<sub>n</sub> UTFs system.

For SP dissolved in GME solution, both the SP-GME and MC-GME (after UV light irradiation) show a very weak emission peak at 410 nm, which is rather similar to that of GME solvent (Figure 1C). No obvious red-fluorescence of these two samples can be observed by the naked eye (Figure 1A). In the presence of PTBEM, however, different results are obtained. The SP@PTBEM micelle solution shows a feeble red-fluorescence; while the MC@PTBEM micelle (after UV light irradiation) displays an extremely strong red emission at 600 nm (Figure 1C). The discrimination can be clearly observed in Figure 1B, and MC@PTBEM micelle shows much stronger fluorescence intensity than MC in various solvents (Figure S5). In addition, the PLQY of MC@PTBEM micelle (5.62%) is significantly enhanced compared with that of pure MC in GME solution (2.69%) (Figure 1D). This is comparable with previously reported results.<sup>36</sup> The results above indicate

**Scheme 1. Schematic Representation for the Fabrication of  $(SP@PTBEM/LDHs)_n$  UTFs via LBL Self-Assembly**  
**Method:** (A) SP, (B) PTBEM, (C) SP@PTBEM Micelle, (D) LDHs Nanoplatelet, (E) Quartz Glass Substrate



that the fluorescence of MC is largely improved in the PTBEM micelle core, which is attributed to the fact that a hydrophobic microenvironment normally enhances the fluorescence intensity of spiropyran.<sup>6,9,37,38</sup> This is particularly important in the following assembly of switchable fluorescent UTFs.

Subsequently, the  $(SP@PTBEM/LDHs)_n$  UTFs were fabricated by assembling SP@PTBEM micelle with LDHs nanoplatelets onto the quartz substrate via the LBL deposition technique. The fluorescence spectra show an emission at 610 nm for these UTFs (Figure 2A); the intensity enhances linearly along with the increase of bilayer number (Figure 2B). This result can be further confirmed by the increased red emission from visual observations (Figure 2A, inset: from  $n = 4$  to 20).

Compared with the SP@PTBEM micelles solution, a red-shift of 10 nm in fluorescence peak is found for the  $(SP@PTBEM/LDHs)_n$  UTJs, indicating that the interaction between LDHs and SP@PTBEM micelle imposes some influence on the photoluminescence behavior of chromophore.<sup>39</sup>

For an intelligent photoresponsive switch, both a strong fluorescence intensity and a fast responsive time are simultaneously required. The relationship between responsive time and bilayer number was therefore studied. Figure 2C displays the time dependence of fluorescence intensity at 610 nm for  $(SP@PTBEM/LDHs)_n$  UTJs under 365 nm excitation, which can be divided into three sections: (1) the rise of fluorescence intensity: UV irradiation induces the structural transformation from closed-ring SP to open-ring MC, resulting in the enhancement of red fluorescence at 610 nm; (2) the state of equilibrium: the maximum emission is obtained at the time point of the largest structural transformation, which is defined as the responsive time; and (3) the decline of fluorescence intensity: continuous irradiation by UV light causes the photobleaching of UTJs and the resulting intensity decrease. Interestingly, the responsive time increases linearly as a function of the bilayer number  $n$  (Figure 2D), implying that a thick film reduces the response sensitivity toward light. Owing to the opposite change of responsive time and fluorescence intensity against film thickness, a reasonable compromise is necessary. Taking into account both of these two factors, the  $(SP@PTBEM/LDHs)_{12}$  UTJ with a relatively strong intensity and a fast response was chosen for further study. The switching time in this work (120 s) measured by a fluorospectrophotometer is comparable with the previously reported value for spiropyran-based material (200 s) under the same experiment conditions.<sup>9</sup> Moreover, it can be further reduced to 15 s by using a high-pressure mercury ultraviolet lamp (8 W).

### 3.2. Structural and Morphological Characterizations.

The surface morphology of  $(SP@PTBEM/LDHs)_{12}$  UTJ was

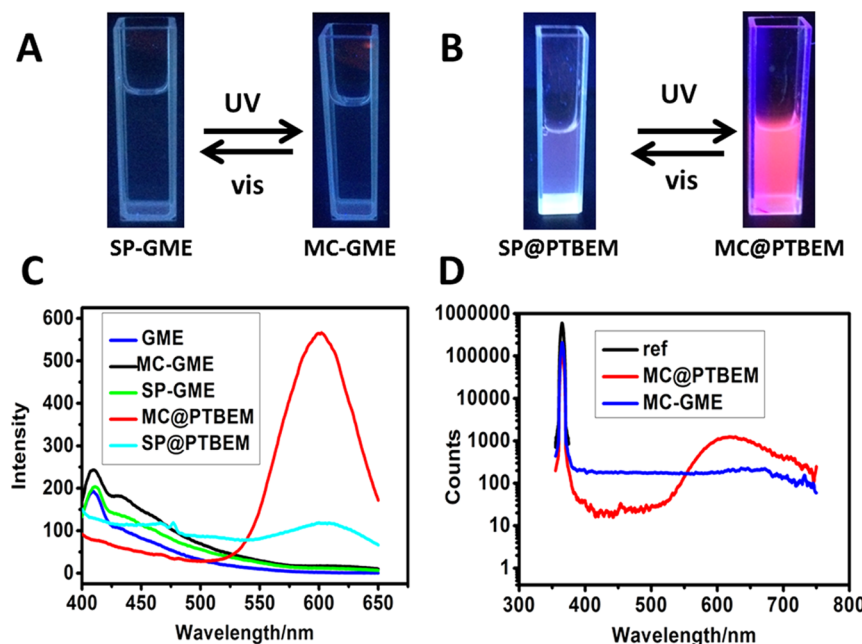


**Figure 1.** Fluorescence photographs of (A) SP and MC in GME solution, and (B) SP@PTBEM and MC@PTBEM micelle solution. (C) Photoluminescence spectra of GME solution, SP in GME solution, MC in GME solution, SP@PTBEM micelle solution, and MC@PTBEM micelle solution ( $\lambda_{ex} = 365$  nm). (D) Quantum yield results for multiscans (excitation range: 355.00–374.80 nm; luminescence range: 450.00–750.00 nm) of MC in GME solution and MC@PTBEM micelle, respectively.

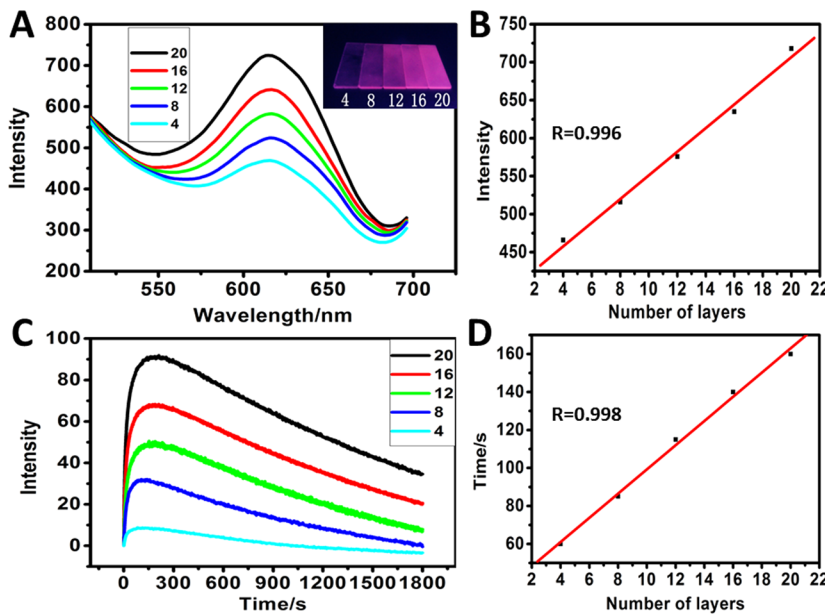


**Figure 2.** (A) Photoemission spectra of  $(\text{SP}@\text{PTBEM}/\text{LDHs})_n$  UTFs from  $n = 4$  to 20; the inset shows the photographs of UTFs under 365 nm UV illumination. (B) The plot of intensity at 610 nm versus  $n$ . (C) Time dependence of the fluorescence intensity at 610 nm for  $(\text{SP}@\text{PTBEM}/\text{LDHs})_n$  UTFs ( $\lambda_{\text{ex}} = 365$  nm). (D) The plot of responsive time as a function of  $n$ .

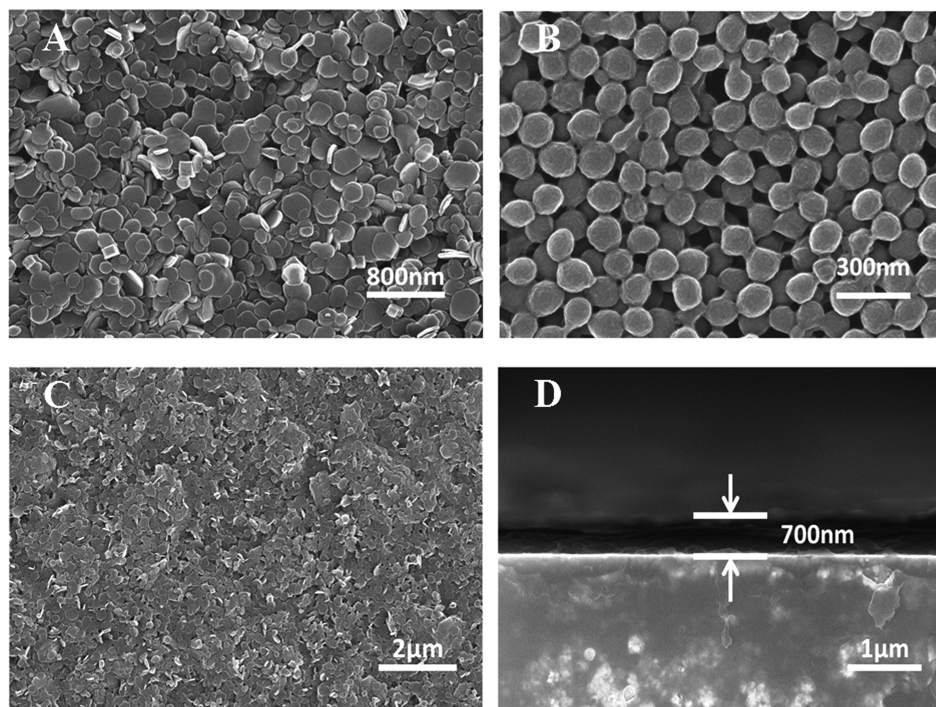


**Figure 3.** SEM images of (A) LDHs nanoplatelets, (B) SP@PTBEM micelles, (C) top-view image of  $(\text{SP}@\text{PTBEM}/\text{LDHs})_{12}$  UTF with LDHs nanoplatelets as the terminal layer, and (D) side-view image of  $(\text{SP}@\text{PTBEM}/\text{LDHs})_{12}$  UTF on a silicon substrate.

investigated by SEM. Figure 3A shows the SEM image of LDHs nanoplatelets, with a hexagonal platelet shape and an average diameter of  $\sim 200$  nm (XRD in Figure S6). The SP@PTBEM micelle is revealed as individual spheric morphology with a uniform diameter of  $\sim 100$  nm (Figure 3B). Figure 3C displays the top-view of  $(\text{SP}@\text{PTBEM}/\text{LDHs})_{12}$  UTF with the LDHs nanoplatelets as the terminal layer, from which a relatively uniform and smooth surface is observed. Side-view SEM image (Figure 3D) gives an estimation on the thickness of  $(\text{SP}@\text{PTBEM}/\text{LDHs})_{12}$  UTF ( $\sim 700$  nm). Moreover, an approx-

imately linear increase of film thickness as a function of  $n$  is observed, with a bilayer thickness of 59 nm (Figure S7, S8).

The variation mechanism from nonfluorescent state to red fluorescence can be ascribed to the structural transformation from closed-ring SP to open-ring MC, in which the change of binding energy for N 1s core level region can be proved by an XPS spectrum. The binding energy of N 1s for SP (indoline nitrogen) and MC ( $\text{N}^+$  species) are located at 399.7 and 402.1 eV, respectively, which offers an effective indication on these two species.<sup>40,41</sup> For the  $(\text{SP}@\text{PTBEM}/\text{LDHs})_{12}$  UTF without

UV illumination, a strong peak at 399.7 eV and a weak one at 402.1 eV are observed (Figure 4A), revealing the coexistence of

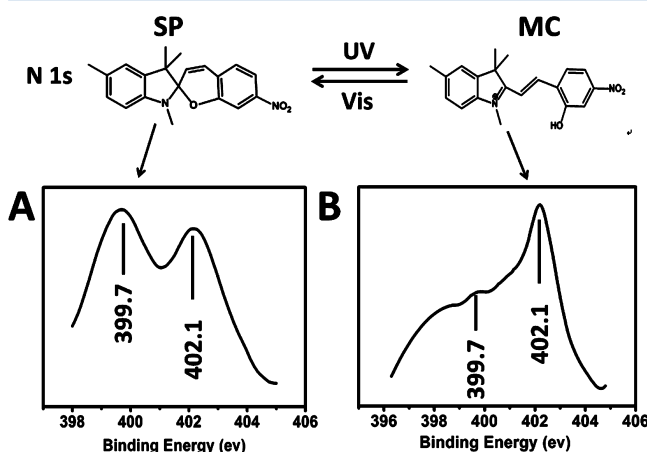


**Figure 4.** X-ray photoemission spectra of the N 1s core level regions of  $(\text{SP}@\text{PTBEM}/\text{LDHs})_{12}$  UTFs for (A) the closed-ringed SP form and (B) open-ringed MC form.

predominant SP and minor MC. This has been reported that the inductive effect of polar solvent (e.g., water and GME) would inevitably lead to partial transformation of SP to MC, accounting for a coexistence state.<sup>32,42</sup> After UV irradiation at 365 nm for 120 s, the N 1s peak at 399.7 eV descends sharply, while the one at 402.1 eV increases significantly (Figure 4B), demonstrating that most SP molecules in the micelle core turn to MC upon UV irradiation.

The lifetime of the fluorophore indicator is a crucial parameter in the evaluation of light-triggered switch. The fluorescence decays of powdered SP, SP in GME solution, SP@PTBEM micelle solution, and  $(\text{SP}@\text{PTBEM}/\text{LDHs})_n$  UTFs with various bilayer numbers were detected at 365 nm excitation (Figure S9). The precise nature of fluorescence decay reflects the interaction details between fluorophores and their environment, and a more accurate fluorescence lifetime ( $\tau$ ) can be obtained when the variance ( $\chi^2$ ) is much closer to 1.000.<sup>43,44</sup> In this work, the single-exponential and double-exponential fitting are performed, respectively, and the later method gives a variance ( $\chi^2$ ) closer to 1.000. Therefore, the double-exponential fitting was used to determine the fluorescence lifetime. The fluorescence lifetime (Table 1) and fluorescence decay curves (Figure S9) reveal that the lifetime of

SP@PTBEM micelle solution is 3.295 ns, 7.5 times longer compared with that of the pristine SP in GME solution (0.449 ns), demonstrating that the micellization improves the stability of excited state of SP. In addition, a longer fluorescence lifetime of the  $(\text{SP}@\text{PTBEM}/\text{LDHs})_n$  UTFs samples (1.976 ns–3.136 ns) is obtained compared with SP powdered sample (1.612 ns), indicating that the confinement effect imposed by the PTBEM micelle and LDHs nanoplatelets enhances the lifetime of excited state species.<sup>45</sup>

**3.3. Photoresponsive Switch Behavior of  $(\text{SP}@\text{PTBEM}/\text{LDHs})_{12}$  UTFs.** The photoresponsive switch behavior of the  $(\text{SP}@\text{PTBEM}/\text{LDHs})_{12}$  UTF was further studied. The peak intensity at 610 nm for the UTF enhances gradually along with the increased time (0–120 s) of UV light irradiation (Figure 5A), which is confirmed by visual observations (Figure 5A,

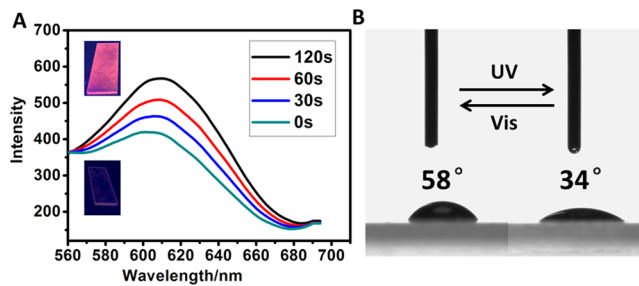


**Figure 5.** (A) Photoemission spectra and photographs of  $(\text{SP}@\text{PTBEM}/\text{LDHs})_{12}$  UTF along with UV irradiation time (0–120 s) ( $\lambda_{\text{ex}} = 365$  nm). (B) Photoinduced change in the contact angle of a water droplet on  $(\text{SP}@\text{PTBEM}/\text{LDHs})_{12}$  UTF.

inset). The intensity can return back to the original state when the UTF is maintained in a daylight environment. A fluorescence microscopy image was used to test the switch behavior, in which a red emission and nonfluorescence can be distinguished upon UV/visible light illumination alternately (Figure S10). In order to study the influence of structural transformation between SP and MC on the surface wettability, the contact angle of water droplet on  $(\text{SP}@\text{PTBEM}/\text{LDHs})_{12}$  UTF was determined. A reversible variation between  $58^\circ$  at  $(\text{SP}@\text{PTBEM}/\text{LDHs})_{12}$  UTF and  $34^\circ$  at  $(\text{MC}@\text{PTBEM}/\text{LDHs})_{12}$  UTF occurs (Figure 5B), showing the hydrophobic and hydrophilic function controlled by UV/visible light.<sup>46,47</sup>

Reversibility and photostability are extremely important criteria in practical applications of light-triggered switches or

**Table 1. Fluorescence Lifetimes of  $(\text{SP}@\text{PTBEM}/\text{LDHs})_n$  UTFs with Double-Exponential Fitting Detected at Their Own Maxima Emission ( $\lambda_{\text{ex}} = 365$  nm)**

|   | $\tau_i$ (ns)  | $Ai$ (%)         | $\tau$ (ns) | $\chi^2$ |
|---|----------------|------------------|-------------|----------|
| SP in GME solution ( $1.5 \times 10^{-3}$ mol·L <sup>-1</sup> ) | 0.102<br>5.512 | 93.56%<br>6.44%  | 0.449       | 1.350    |
| SP@PTBEM micelle solution                                       | 1.519<br>4.442 | 39.24%<br>60.76% | 3.295       | 1.205    |
| SP powdered sample  | 1.324<br>3.133 | 84.07%<br>15.93% | 1.612       | 1.225    |
| $(\text{SP}@\text{PTBEM}/\text{LDHs})_2$                        | 0.925<br>3.306 | 55.87%<br>44.13% | 1.976       | 1.175    |
| $(\text{SP}@\text{PTBEM}/\text{LDHs})_{12}$                     | 0.854<br>3.335 | 53.42%<br>46.58% | 2.231       | 1.194    |
| $(\text{SP}@\text{PTBEM}/\text{LDHs})_{20}$                     | 1.575<br>4.521 | 45.83%<br>54.17% | 3.136       | 1.175    |

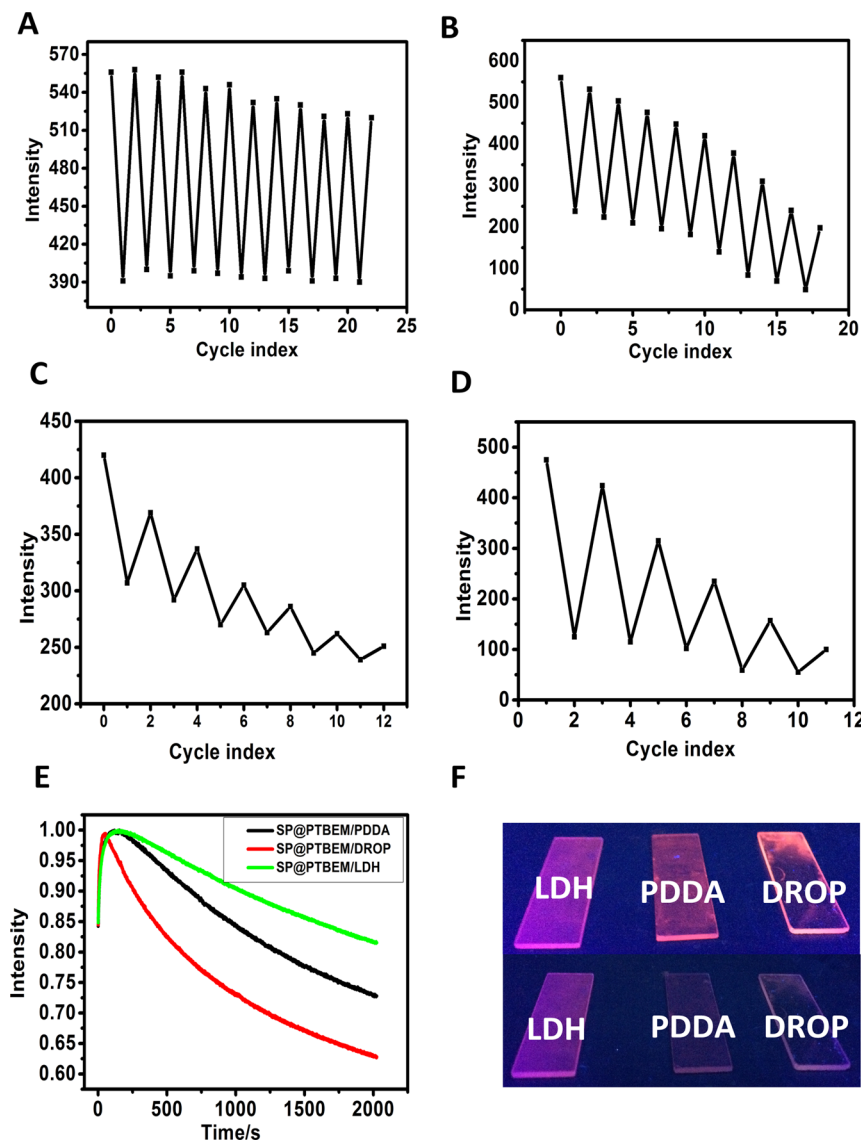


**Figure 6.** Reversibility recorded by alternate irradiation upon UV/visible light for several cycles: (A)  $(\text{SP}@\text{PTBEM}/\text{LDHs})_{12}$  UTF, (B)  $\text{SP}@\text{PTBEM}$  micelles solution, (C)  $(\text{SP}@\text{PTBEM}/\text{PDDA})_{12}$  UTF, (D)  $(\text{SP}@\text{PTBEM}/\text{DROP})$  UTF. (E) Time dependence of the fluorescence intensity at 610 nm upon UV illumination:  $(\text{SP}@\text{PTBEM}/\text{LDHs})$ ,  $(\text{SP}@\text{PTBEM}/\text{PDDA})$ , and  $(\text{SP}@\text{PTBEM}/\text{DROP})$  UTF. (F) Photographs of three UTFs under 365 nm UV illumination at  $t = 0$  (up) and  $t = 2000\text{s}$  (down), respectively.

optoelectronic devices. The reversibility of  $(\text{SP}@\text{PTBEM}/\text{LDHs})_{12}$  UTF was investigated by alternate UV/visible light irradiation for several cycles, in comparison with the following control samples:  $\text{SP}@\text{PTBEM}$  micelle solution,  $(\text{SP}@\text{PTBEM}/\text{PDDA})_{12}$  UTF and  $(\text{SP}@\text{PTBEM}/\text{DROP})$  UTF. The  $(\text{SP}@\text{PTBEM}/\text{LDHs})_{12}$  UTF possesses the best reversibility: its fluorescence intensity at 610 nm remains at 90% after 11 consecutive cycles (Figure 6A). In contrast, the emission at 610 nm for all the three control samples decreases sharply (Figure 6B,C,D). The photostability of the  $(\text{SP}@\text{PTBEM}/\text{LDHs})_{12}$  UTF was further studied by continuous illuminating with UV light, compared with  $(\text{SP}@\text{PTBEM}/\text{PDDA})_{12}$  and  $(\text{SP}@\text{PTBEM}/\text{DROP})$  UTF. After a 2000 s irradiation, the fluorescent intensity (610 nm) of  $(\text{SP}@\text{PTBEM}/\text{PDDA})_{12}$  and  $(\text{SP}@\text{PTBEM}/\text{DROP})$  UTF decreases 27% and 38%, respectively; while only 15% loss is found for the  $(\text{SP}@\text{PTBEM}/\text{LDHs})_{12}$  UTF (Figure 6E). A significant comparison of photostability was provided by visual observations (Figure 6F). The results indicate that both the reversibility and

photostability are significantly improved by incorporation of SP in this organic–inorganic UTF system. The loss in reversibility and photostability of pristine SP is attributed to the interaction of the long-lived triplet excited state of SP with singlet oxygen ( ${}^1\text{O}_2$ ) and the resulting irreversible oxidation;<sup>48,49</sup> therefore, SP-based switching was usually carried out in an airtight environment.<sup>50</sup> In this work, both the LDHs nanoplatelets and PTBEM micelles provide an airtight architecture to protect SP from contacting with oxygen, accounting for the largely enhanced reversibility and photostability of  $(\text{SP}@\text{PTBEM}/\text{LDHs})_{12}$  UTF.<sup>51</sup>

#### 4. CONCLUSION

In conclusion, a photoresponsive switch was designed and fabricated based on  $\text{SP}@\text{PTBEM}$  micelle and LDHs nanoplatelets via a two-step procedure. The UTFs exhibit a periodic long-range stacking order structure and controllable photoemission intensity. The luminescence color of the resulting hybrid UTFs can be easily tuned between nonfluorescent

closed-ring SP and red-fluorescent open-ring MC by alternate UV/visible light irradiation, allowing a fast light-triggered switch. A high reversibility and photostability was demonstrated for the  $(\text{SP}@\text{PTBEM}/\text{LDHs})_{12}$  UTF, as a result of the confinement effect imposed by PTBEM micelle and LDHs matrix. It is anticipated that the strategy demonstrated in this work can be extended to the fabrication of other photoresponsive switches with unique functionality, which would facilitate potential applications in displays, sensors, and optoelectronic devices.

## ■ ASSOCIATED CONTENT

### Supporting Information

Synthesis of spiropyran ( $\text{C}_{20}\text{H}_{20}\text{N}_2\text{O}_3$ ) (Figure S1–S4, Scheme S1–S2); fluorescence photographs and photoluminescence spectra of spiropyrane in various solvents (Figure S5); XRD pattern of MgAl-LDHs nanoplatelets (Figure S6); thickness of  $(\text{SP}@\text{PTBEM}/\text{LDHs})_n$  UTFs (Figure S7–S8), fluorescence decay curves (Figure S9); fluorescence microscopy image of the  $(\text{SP}@\text{PTBEM}/\text{LDHs})_{12}$  UTFs (Figure S10). This material is available free of charge via the Internet at <http://pubs.acs.org>.

## ■ AUTHOR INFORMATION

### Corresponding Authors

\*Fax: +86-10-64425385; Tel: +86-10-64412131; E-mail: weimin@mail.buct.edu.cn (M.W.).

\*E-mail: yinmz@mail.buct.edu.cn (M.Y.).

### Notes

The authors declare no competing financial interest.

## ■ ACKNOWLEDGMENTS

This work was supported by the 973 Program (Grant No.: 2014CB932104), the National Natural Science Foundation of China (NSFC), the Scientific Fund from Beijing Municipal Commission of Education, and the Fundamental Research Funds for the Central Universities (YS1406). M.W. appreciates the China National Funds for Distinguished Young Scholars of the NSFC.

## ■ REFERENCES

- Raymo, F. M.; Alvarado, R. J.; Giordani, S.; Cejas, M. A. Memory Effects Based on Intermolecular Photoinduced Proton Transfer. *J. Am. Chem. Soc.* **2003**, *125*, 2361–2364.
- Zacharias, P.; Gather, M. C.; Koehnen, A.; Rehmann, N.; Meerholz, K. Photoprogrammable Organic Light-Emitting Diodes. *Angew. Chem., Int. Ed.* **2009**, *48*, 4038–4041.
- Hu, D.; Tian, Z.; Wu, W.; Wan, W.; Li, A. D. Q. Photoswitchable Nanoparticles Enable High-Resolution Cell Imaging: PULSAR Microscopy. *J. Am. Chem. Soc.* **2008**, *130*, 15279–15281.
- Wu, W.; Yao, L.; Yang, T.; Yin, R.; Li, F.; Yu, Y. NIR-Light-Induced Deformation of Cross-Linked Liquid-Crystal Polymers Using Upconversion Nanophosphors. *J. Am. Chem. Soc.* **2011**, *133*, 15810–15813.
- Liu, Q.; Peng, J.; Sun, L.; Li, F. High-Efficiency Upconversion Luminescent Sensing and Bioimaging of Hg (II) by Chromophoric Ruthenium Complex-Assembled Nanophosphors. *ACS Nano* **2011**, *5*, 8040–8048.
- Klajn, R. Spiropyran-Based Dynamic Materials. *Chem. Rev.* **2014**, *43*, 148–184.
- Minkin, V. I. Photo-, Thermo-, Solvato-, and Electrochromic Spiroheterocyclic Compounds. *Chem. Rev.* **2004**, *104*, 2751–2776.
- Garry, B.; Valeri, K.; Victor, W. Spiropyrans and Spirooxazines for Memories and Switches. *Chem. Rev.* **2000**, *100*, 1741–1754.
- Zhu, M.-Q.; Zhang, G.-F.; Li, C.; Aldred, M. P.; Chang, E.; Drezek, R. A.; Li, A. D. Q. Reversible Two-Photon Photoswitching and Two-Photon Imaging of Immunofunctionalized Nanoparticles Targeted to Cancer Cells. *J. Am. Chem. Soc.* **2011**, *133*, 365–372.
- Li, C.; Zhang, Y.; Hu, J.; Cheng, J.; Liu, S. Reversible Three-State Switching of Multicolor Fluorescence Emission by Multiple Stimuli Modulated FRET Processes within Thermoresponsive Polymeric Micelles. *Angew. Chem., Int. Ed.* **2010**, *49*, 5120–5124.
- Zhu, L. Y.; Zhu, M. Q.; Hurst, J. K.; Li, A. D. Q. Light-Controlled Molecular Switches Modulate Nanocrystal Fluorescence. *J. Am. Chem. Soc.* **2005**, *127*, 8968–8970.
- Chen, J.; Zeng, F.; Wu, S.; Zhao, J.; Chen, Q.; Tong, Z. Reversible Fluorescence Modulation Through Energy Transfer with ABC Triblock Copolymer Micelles as Scaffolds. *Chem. Commun.* **2008**, *44*, 5580–5582.
- Liao, B.; Long, P.; He, B.; Yi, S.; Ou, B.; Shen, S.; Chen, J. Reversible Fluorescence Modulation of Spiropyran-Functionalized Carbon Nanoparticles. *J. Mater. Chem. C* **2013**, *1*, 3716–3721.
- Florea, L.; McKeon, A.; Diamond, D.; Benito-Lopez, F. Spiropyran Polymeric Microcapillary Coatings for Photodetection of Solvent Polarity. *Langmuir* **2013**, *29*, 2790–2797.
- Bambang, K.; Narayanaswamy, R. Polymeric Encapsulated Membrane for Optrodes. *J. Anal. Chem.* **1999**, *364*, 605–607.
- Buchholz, K.; Buschmann, N.; Cammann, K. A Fibre-Optical Sensor for the Determination of Sodium with a Reversible Response. *Sens. Actuator. B* **1992**, *9*, 41–47.
- Wang, Q.; O'Hare, D. Recent Advances in the Synthesis and Application of Layered Double Hydroxide (LDH) Nanosheets. *Chem. Rev.* **2012**, *112*, 4124–4155.
- Williams, G. R.; Fogg, A. M.; Sloan, J.; Taviot-Gueho, C.; O'Hare, D. Staging During Anion-Exchange Intercalation into  $[\text{LiAl}_2(\text{OH})_6]\text{Cl}\cdot y\text{H}_2\text{O}$ : Structural and Mechanistic Insights. *Dalton Trans.* **2007**, *32*, 3499–3506.
- Darder, M.; Lopez-Blanco, M.; Aranda, P.; Leroux, F.; Ruiz-Hitzky, E. Bio-Nanocomposites Based on Layered Double Hydroxides. *Chem. Mater.* **2005**, *17*, 1969–1977.
- Williams, G. R.; O'Hare, D. Towards Understanding, Control and Application of Layered Double Hydroxide Chemistry. *J. Mater. Chem.* **2006**, *16*, 3065–3074.
- Liu, Z. P.; Ma, R. Z.; Osada, M.; Iyi, N.; Ebina, Y.; Takada, K.; Sasaki, T. Synthesis, Anion Exchange, and Delamination of Co-Al Layered Double Hydroxide: Assembly of the Exfoliated Nanosheet/Polyanion Composite Films and Magneto-Optical Studies. *J. Am. Chem. Soc.* **2006**, *128*, 4872–4880.
- Vucelic, M.; Moggridge, G. D.; Jones, W. Thermal Properties of Terephthalate- and Benzoate-Intercalated LDH. *J. Phys. Chem.* **1995**, *99*, 8328–8337.
- Kang, H.; Huang, G.; Ma, S.; Bai, Y.; Ma, H.; Li, Y.; Yang, X. Coassembly of Inorganic Macromolecule of Exfoliated LDH Nanosheets with Cellulose. *J. Phys. Chem. C* **2009**, *113*, 9157–9163.
- Leroux, F.; Taviot-Gueho, C. Fine Tuning Between Organic and Inorganic Host Structure: New Trends in Layered Double Hydroxide Hybrid Assemblies. *J. Mater. Chem.* **2005**, *15*, 3628–3642.
- Desigaux, L.; Ben Belkacem, M.; Richard, P.; Cellier, J.; Leone, P.; Cario, L.; Leroux, F.; Taviot-Gueho, C.; Pitard, B. Self-Assembly and Characterization of Layered Double Hydroxide/DNA Hybrids. *Nano Lett.* **2006**, *6*, 199–204.
- Fogg, A. M.; Freij, A. J.; Parkinson, G. M. Synthesis and Anion Exchange Chemistry of Rhombohedral Li/Al Layered Double Hydroxides. *Chem. Mater.* **2002**, *14*, 232–234.
- Yan, D.; Lu, J.; Wei, M.; Han, J.; Ma, J.; Li, F.; Evans, D. G.; Duan, X. Ordered poly(p-phenylene)/Layered Double Hydroxide Ultrathin Films with Blue Luminescence by Layer-by-Layer Assembly. *Angew. Chem., Int. Ed.* **2009**, *48*, 3073–3076.
- Yan, D.; Lu, J.; Ma, J.; Wei, M.; Evans, D. G.; Duan, X. Reversibly Thermochromic, Fluorescent Ultrathin Films with a Supramolecular Architecture. *Angew. Chem., Int. Ed.* **2011**, *50*, 720–723.

- (29) Zhang, M.; Han, D.; Lu, C.; Lin, J.-M. Organo-Modified Layered Double Hydroxides Switch-On Chemiluminescence. *J. Phys. Chem. C* **2012**, *116*, 6371–6375.
- (30) Qin, Y.; Lu, J.; Li, S.; Li, Z.; Zheng, S. Phosphorescent Sensor Based on Iridium Complex/Poly(vinylcarbazole) Orderly Assembled with Layered Double Hydroxide Nanosheets: Two-Dimensional Foster Resonance Energy Transfer and Reversible Luminescence Response for VOCs. *J. Phys. Chem. C* **2014**, *118*, 20538–20544.
- (31) Gunawan, P.; Xu, R. Lanthanide-Doped Layered Double Hydroxides Intercalated with Sensitizing Anions: Efficient Energy Transfer between Host and Guest Layers. *J. Phys. Chem. C* **2009**, *113*, 17206–17214.
- (32) Tian, H.; Feng, Y. Next Step of Photochromic Switches? *J. Mater. Chem.* **2008**, *18*, 1617–1622.
- (33) Henzl, J.; Mehlhorn, M.; Gawronski, H.; Rieder, K. H.; Morgenstern, K. Reversible Cis–Trans Isomerization of a Single Azobenzene Molecule. *Angew. Chem., Int. Ed.* **2006**, *45*, 603–606.
- (34) Fuss, W.; Kosmidis, C.; Schmid, W. E.; Trushin, S. A. The Photochemical Cis–Trans Isomerization of Free Stilbene Molecules Follows a Hula-Twist Pathway. *Angew. Chem., Int. Ed.* **2004**, *43*, 4178–4182.
- (35) Tian, Z.; Wu, W.; Wan, W.; Li, A. D. Q. Photoswitching-Induced Frequency-Locked Donor–Acceptor Fluorescence Double Modulations Identify the Target Analyte in Complex Environments. *J. Am. Chem. Soc.* **2011**, *133*, 16092–16100.
- (36) Jeffrey, W.; Corinne, B.; Veronique, M. Photodynamic Fluorescent Metal Ion Sensors with Parts per Billion Sensitivity. *J. Am. Chem. Soc.* **1998**, *120*, 3237–3242.
- (37) Huang, C. Q.; Wang, Y.; Hong, C. Y.; Pan, C. Y. Spiropyran-Based Polymeric Vesicles: Preparation and Photochromic Properties. *Macromol. Rapid Commun.* **2011**, *32*, 1174–1179.
- (38) Chan, Y.-H.; Gallina, M. E.; Zhang, X.; Wu, I. C.; Jin, Y.; Sun, W.; Chiu, D. T. Reversible Photoswitching of Spiropyran-Conjugated Semiconducting Polymer Dots. *Anal. Chem.* **2012**, *84*, 9431–9438.
- (39) Liang, R.; Xu, S.; Yan, D.; Shi, W.; Tian, R.; Yan, H.; Wei, M.; Evans, D. G.; Duan, X. CdTe Quantum Dots/Layered Double Hydroxide Ultrathin Films with Multicolor Light Emission via Layer-by-Layer Assembly. *Adv. Funct. Mater.* **2012**, *22*, 4940–4948.
- (40) Ivashenko, O.; van Herpt, J. T.; Feringa, B. L.; Rudolf, P.; Browne, R. B. UV/Vis and NIR Light-Responsive Spiropyran Self-Assembled Monolayers. *Langmuir* **2013**, *29*, 4290–4297.
- (41) Pigois, E.; Gayot, D.; Delamar, M.; Leclerc, M.; Chehimi, M. M. X-ray Photoelectron Spectroscopy of Spiropyran Molecules. *J. Electron Spectrosc. Relat. Phenom.* **1990**, *53*, 79–86.
- (42) Rosario, R.; Gust, D.; Hayes, M.; Jahnke, F.; Springer, J.; Garcia, A. A. Photon-Modulated Wettability Changes on Spiropyran-Coated Surfaces. *Langmuir* **2002**, *18*, 8062–8069.
- (43) Stephen, D. S.; Joakim, A.; Gerdenis, K.; Ana, L. M.; Thomas, A. M.; Devens, G. Photochromic Control of Photoinduced Electron Transfer Molecular Double-Throw Switch. *J. Am. Chem. Soc.* **2005**, *127*, 2717–2724.
- (44) Wei, L.; Na, L.; Yu, L. L.; Ye, L.; An, D. X. Shape-Specific Detection Based on Fluorescence Resonance Energy Transfer Using a Flexible Water-Soluble Conjugated Polymer. *J. Am. Chem. Soc.* **2006**, *128*, 10281–10287.
- (45) Shi, W.; He, S.; Wei, M.; Evans, D. G.; Duan, X. Optical pH Sensor with Rapid Response Based on a Fluorescein-Intercalated Layered Double Hydroxide. *Adv. Funct. Mater.* **2010**, *20*, 3856–3863.
- (46) Samanta, S.; Locklin, J. Formation of Photochromic Spiropyran Polymer Brushes via Surface-Initiated, Ring-Opening Metathesis Polymerization: Reversible Photocontrol of Wetting Behavior and Solvent Dependent Morphology Changes. *Langmuir* **2008**, *24*, 9558–9565.
- (47) Wang, D.; Jiao, P.; Wang, J.; Zhang, Q.; Feng, L.; Yang, Z. Fast Photo-Switched Wettability and Color of Surfaces Coated with Polymer Brushes Containing Spiropyran. *J. Appl. Polym. Sci.* **2012**, *125*, 870–875.
- (48) Baillet, G.; Giusti, G.; Guglielmetti, R. Comparative Photo-degradation Study Between Spiro[Indoline-Oxazine] and Spiro[Indoline-Pyran] Derivatives in Solution. *J. Photochem. Photobiol., A* **1993**, *70*, 157–161.
- (49) Baillet, G.; Campredon, M.; Guglielmetti, R.; Giusti, G.; Aubert, C. Dealkylation of N-Substituted Indolinospironaphthoxazine Photochromic Compounds under UV Irradiation. *J. Photochem. Photobiol., A* **1994**, *83*, 147–151.
- (50) Matsushima, R.; Nishiyama, M.; Doi, M. Improvements in the Fatigue Resistances of Photochromic Compounds. *J. Photochem. Photobiol., A* **2001**, *139*, 63–69.
- (51) Chakraborty, C.; Dana, K.; Malik, S. Intercalation of Perylenediimide Dye into LDH Clays: Enhancement of Photostability. *J. Phys. Chem. C* **2011**, *115*, 1996–2004.